

Article

Thermal–Structural Linear Static Analysis of Functionally Graded Beams Using Reddy Beam Theory

Carlos Enrique Valencia Murillo , Miguel Ernesto Gutierrez Rivera *  and Luis David Celaya Garcia 

Department of Mechanical Engineering, University of Guanajuato, Salamanca 36885, Mexico; ce.valenciamurillo@ugto.mx (C.E.V.M.); ld.celayagarcia@ugto.mx (L.D.C.G.)

* Correspondence: miguel.gutierrez@ugto.mx

Abstract: In this work, a finite element model to perform the thermal–structural analysis of beams made of functionally graded material (FGM) is presented. The formulation is based on the third-order shear deformation theory. The constituents of the FGM are considered to vary only in the thickness direction, and the effective material properties are evaluated by means of the rule of mixtures. The volume distribution of the top constituent is modeled using the power law form. A comparison of the present finite element model with the numerical results available in the literature reveals that they are in good agreement. In addition, a routine to study functionally graded plane models in a commercial finite element code is used to verify the performance of the proposed model. In the present work, displacements for different values of the power law exponent and surface temperatures are presented. Furthermore, the normal stress variation along the thickness is shown for several power law exponents of functionally graded beams subjected to thermal and mechanical loads.

Keywords: beam; thermal analysis; third-order shear deformation theory; functionally graded material; finite element model



Citation: Valencia Murillo, C.E.; Gutierrez Rivera, M.E.; Celaya Garcia, L.D. Thermal–Structural Linear Static Analysis of Functionally Graded Beams Using Reddy Beam Theory. *Math. Comput. Appl.* **2023**, *28*, 84. <https://doi.org/10.3390/mca28040084>

Academic Editor: Nicholas Fantuzzi, Michele Baccocchi, Eugenio Ruocco, Maria Amélia Ramos Loja and Jose Antonio Loya

Received: 30 June 2023
Revised: 20 July 2023
Accepted: 21 July 2023
Published: 23 July 2023



Copyright: © 2023 by the authors. Licensee MDPI, Basel, Switzerland. This article is an open access article distributed under the terms and conditions of the Creative Commons Attribution (CC BY) license (<https://creativecommons.org/licenses/by/4.0/>).

1. Introduction

Functionally graded materials (FGMs) are advanced materials made from a mixture of two or more constituents, and, therefore, they are not homogeneous. Typically, the mixture consists of a ceramic and a metallic material, and it is designed to have a continuous variation in material composition. The gradient of material properties allows the reduction of thermal and residual stresses, as well as the stress concentrations presented in laminated composite materials [1–5].

FGMs are often used in structures or applications that commonly operate under extreme temperature and/or environmental conditions, such as spacecrafts, aircrafts, and nuclear reactors [6–8]. The main reasons for their use are their outstanding thermo-mechanical properties, corrosion resistance, and high fracture toughness [9].

Many of the structural elements or components operating under these extreme environments are beams. For that reason, it is important to analyze the behavior of these types of elements [6]. Since the beam element is one of the most used in structural analysis, there are several theories available to describe its mechanical behavior. Among these are Euler–Bernoulli beam theory or classical beam theory (CBT), Timoshenko beam theory or first-order shear deformation theory (FSDT), Reddy–Bickford beam theory or third-order shear deformation theory (TSDT), and other higher-order shear deformation theories (HSDTs).

Static, dynamic, and modal analyses of functionally graded beams under mechanical loads have been made using these theories. Li [10] presented a unified approach to analyze the static and dynamic behavior of functionally graded beams (FGB), where the Euler–Bernoulli beam theory could be reduced from the Timoshenko beam theory as a special case. Alshorbagy et al. [11] investigated the free vibration response of FGB by means of the finite element method and the CBT. Moheimani and Ahmadian [12] studied the free

vibration response of FGB using the Euler–Bernoulli beam theory and the non-local theory of elasticity. Chakraborty et al. [1] performed static and free vibration analyses of FGB using the FSDT. Nguyen et al. [13] studied the static and free vibration responses of axially loaded rectangular FGB using the FSDT. A higher-order finite element, based on the unified and integrated approach of Timoshenko beam theory, was developed by Katili et al. [14]. They performed static and free vibration analyses of FGB. Kadoli et al. [15] presented the static analysis of FGB using the TSDT. The free vibration of FGB was investigated by Aydogdu and Taskin [16] by means of a Navier-type solution method and different higher-order shear deformation theories. Mahi et al. [17] developed an exact model to study the free vibration response of FGB using a unified HSDT, where the material properties were taken as temperature-dependent. Thai and Vo [18] used different HSDTs to study the bending and free vibration of FGB. A similar analysis was made later by Vo et al. [19] using only a refined shear deformation theory. Şimşek and Reddy [20] studied the static bending and free vibration of functionally graded (FG) microbeams using a unified higher-order theory that contained various other theories by introducing a function into the displacement field that characterized the transverse shear and stress distribution along the thickness of the beam. Gao and Zhang [21] developed a non-classical third-order shear deformation beam theory for Reddy–Levinson beams using a modified couple stress theory and a surface elasticity theory that allowed them to consider the beam’s microstructure, surface energy, and Poisson’s effect.

The responses of functionally graded beams under thermal and mechanical loads have also been explored. Chakraborty and Gopalakrishnan [22] analyzed the wave propagation behavior of FGB subjected to high-frequency thermal or mechanical impulses using the spectral finite element method. Daneshmehr et al. [23] developed a micro-scale Reddy beam model based on the couple stress theory to analyze the thermal effect on the vibration, buckling, and static bending analyses. They obtained solutions using series expansions for the generalized displacements, which satisfied the boundary conditions. El-Megharbel [9] performed a theoretical analysis of FGB under thermal loads. De Pietro et al. [7] studied the thermo-elastic response of FGB using Carrera’s unified formulation. Lim and Kim [24] used the FSDT to analyze the behavior of FGB with temperature-dependent material properties. Ebrahimi and Jafari [3] proposed a refined shear deformation beam theory for the thermo-mechanical analysis of FGB with porosities exposed to different thermal loads.

In this paper, a thermal-structural analysis of FGB is presented. The finite element model is developed using the TSDT. The material properties vary through the thickness according to the power law, and the temperature distribution along the same direction is obtained by means of a polynomial series. To verify the behavior of the present finite element model, plane models are developed using ANSYS APDL. Finally, to illustrate the performance of the model, some case studies are reported, where the power law exponent and the difference in the temperature between the top and bottom surfaces are varied.

2. Thermal–Structural Problem Description

To develop the present finite element model of FG beams under thermal and mechanical loads, the following conditions are considered:

- The FG beam has a rectangular cross-section of width b and thickness t , as shown in Figure 1, and the beam’s length is L .
- The top and bottom surfaces, as seen in Figure 1, are exposed to the temperatures T_{top} and T_{bot} , respectively, where $T_{top} > T_{bot}$. The temperature only varies through the z coordinate, and it remains constant along the other directions.
- There is no internal heat generation, and convection heat transfer between the beam’s surfaces and the surrounding media is not considered.
- In this case, a uniform distributed load q_0 is applied to the FG beam, as shown in Figure 1. However, the distributed load can also be function of the x coordinate.

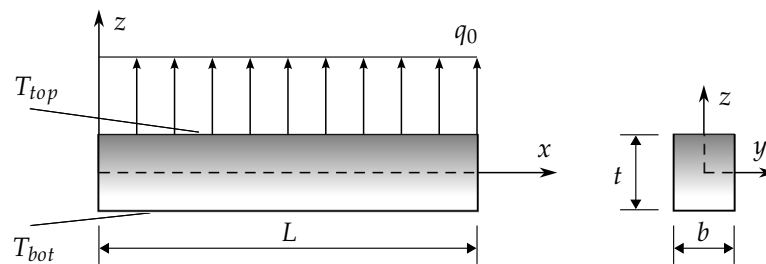


Figure 1. FG beam subjected to a distributed load with different temperatures of the top and bottom surfaces.

2.1. Mechanical Properties

In order to model the variation in the mechanical properties with the variation in the thickness of the beam, Voight’s rule of mixtures is used [25], as follows:

$$P(z) = (P_{top} - P_{bot})V_{top}(z) + P_{bot}, \tag{1}$$

where P denotes the material property and the subscripts top and bot refer to the top and bottom constituent, respectively. $V_{top}(z)$ corresponds to the volume distribution of the top constituent through the thickness of the beam, which is defined by the power law as

$$V_{top}(z) = \left(\frac{2z + t}{2t}\right)^n, \tag{2}$$

where n is the power law exponent, which takes positive values.

2.2. Temperature Distribution

Following the assumptions stated in the problem description of Section 2, the governing equation of the heat transfer through the thickness of the beam is given by

$$\frac{\partial}{\partial z} \left[K(z) \frac{\partial T(z)}{\partial z} \right] = 0, \quad -t/2 \leq z \leq t/2, \tag{3}$$

where $K(z)$ corresponds to the thermal conductivity, and it is calculated using Equation (1). In addition, the boundary conditions are

$$T(-t/2) = T_{bot}, \quad T(t/2) = T_{top}.$$

A solution to the above one-dimensional heat transfer equation was reported in the work of Javaheri and Eslami [26], and it is given as

$$T(z) = T_{bot} + \frac{T_{top} - T_{bot}}{H} \sum_{i=0}^{\eta} \left(\frac{1}{in + 1}\right) \left(\frac{K_{bot} - K_{top}}{K_{bot}}\right)^i \left(\frac{2z + t}{2t}\right)^{(in+1)}, \tag{4}$$

with

$$H = \sum_{i=0}^{\eta} \left(\frac{1}{in + 1}\right) \left(\frac{K_{bot} - K_{top}}{K_{bot}}\right)^i,$$

where i indicates the index of the sum and η denotes the number of terms used in the series for the approximation. One should also remember that n corresponds to the power law exponent presented previously in Equation (2).

3. Finite Element Model

This section briefly presents the development of the finite element model based on the TSDT. In order to obtain the equations for the present model (i.e., the stiffness matrix and

generalized force vector), the definitions for the displacement field, strains, and constitutive equations are required. The displacement field of the TSDT is given by [27,28]

$$u_1(x) = u^0(x) + z\phi^0(x) - \kappa z^3 \left[\phi^0(x) + \frac{\partial w^0(x)}{\partial x} \right], \tag{5}$$

$$u_3(x) = w^0(x), \tag{6}$$

where u^0 is the axial displacement, w^0 is the transverse displacement, ϕ^0 is the rotation of a point located at the centroidal axis x of the beam, and

$$\kappa = \frac{4}{3t^2}. \tag{7}$$

Considering the displacement field of Equations (5) and (6), the nonzero mechanical strains are defined as follows:

$$\epsilon_{11}^M = \frac{\partial u^0}{\partial x} + z \frac{\partial \phi^0}{\partial x} - \kappa z^3 \left(\frac{\partial \phi^0}{\partial x} + \frac{\partial^2 w^0}{\partial x^2} \right) \tag{8}$$

$$\gamma_{13}^M = \phi^0 - 3\kappa z^2 \left(\phi^0 + \frac{\partial w^0}{\partial x} \right) + \frac{\partial w^0}{\partial x}. \tag{9}$$

where, for the sake of brevity, the x argument has been omitted and the superscript M stands for mechanical. On the other hand, the nonzero thermal strain is defined as

$$\epsilon_{11}^T = \alpha(z) [T(z) - T_{ref}], \tag{10}$$

where $\alpha(z)$ denotes the thermal expansion coefficient, and its value is computed by means of the rule of mixtures defined in Equation (1). $T(z)$ is calculated using Equation (4), T_{ref} is the reference temperature at which the material is free of stress, and the superscript T stands for thermal.

Now, the constitutive equations are defined, i.e., the relation between stress and strain. In this case, the stresses, including thermal and mechanical effects, are considered to be defined by

$$\sigma_{11} = \sigma_{11}^M - \sigma_{11}^T, \quad \tau_{13} = \tau_{13}^M, \tag{11}$$

where

$$\sigma_{11}^M = E(z)\epsilon_{11}^M, \quad \sigma_{11}^T = E(z)\epsilon_{11}^T, \quad \tau_{13}^M = G(z)\gamma_{13}^M, \tag{12}$$

where $E(z)$ represents Young's modulus and $G(z)$ is the shear modulus, which is defined as $G(z) = \frac{E(z)}{2(1 + \nu(z))}$, where $\nu(z)$ is Poisson's ratio.

3.1. Principle of Virtual Work

Here, to obtain the stiffness matrix and the force vector involved in the finite element model, the following definition of the principle of virtual work is used:

$$\delta W_I - \delta W_E = 0, \tag{13}$$

where δW_I is the virtual work carried out by internal forces and δW_E is the virtual work carried out by external forces, which are defined by the following expressions:

$$\delta W_I = \int_V \delta \epsilon \cdot \sigma \, dV, \quad \delta W_E = \int_{I^e} \mathbf{f} \cdot \delta \mathbf{u} \, dx, \tag{14}$$

where \mathbf{f} represents the vector associated with the external loads.

For the present model, introducing the strains and stresses defined in Equations (8)–(11) into Equation (14), the following expressions for the virtual works are found:

$$\delta W_I = \int_V \left[\delta \varepsilon_{11}^M E(z) \varepsilon_{11}^M + \delta \gamma_{13}^M G(z) \gamma_{13}^M - \delta \varepsilon_{11}^M E(z) \varepsilon_{11}^T \right] dV, \tag{15}$$

and

$$\delta W_E = \int_{h^e} q_0 \delta w^0(x) dx, \tag{16}$$

where h^e represents the one-dimensional domain of the element.

At this point, all the definitions required to obtain the equations involved in the finite element model have been introduced. In the following sections, the displacement vector, the stiffness matrix, and the generalized force vector are obtained.

3.2. Displacement Vector

In order to obtain the finite element model, the displacement field is approximated as follows:

$$u_j^0 = \sum_{j=0}^p \psi_j^u \Delta_j^{(1)}, \quad w_j^0 = \sum_{j=0}^m \psi_j^w \Delta_j^{(2)}, \quad \phi_k^0 = \sum_{k=0}^p \psi_k^\phi \Delta_k^{(3)}, \tag{17}$$

where the functions ψ_j^u and ψ_k^ϕ correspond to the linear Lagrange polynomials and the function ψ_j^w represents the Hermite cubic interpolation functions. Moreover, $\Delta_j^{(1)}$, $\Delta_j^{(2)}$, and $\Delta_k^{(3)}$ are nodal displacements associated with axial displacement, transverse displacement, and rotation, respectively. In this manner, the displacement vector of the finite element model has the form

$$\Delta = \left[\Delta^{(1)} \quad \Delta^{(2)} \quad \Delta^{(3)} \right]^T. \tag{18}$$

3.3. Stiffness Matrix and Generalized Force Vector

Substituting the strains and stresses into Equation (15) and then replacing the displacements by their approximations defined by Equation (17), the stiffness matrix is found to have the form

$$\mathbf{K}^e = \begin{bmatrix} \mathbf{K}^{11} & \mathbf{K}^{12} & \mathbf{K}^{13} \\ \mathbf{K}^{21} & \mathbf{K}^{22} & \mathbf{K}^{23} \\ \mathbf{K}^{31} & \mathbf{K}^{32} & \mathbf{K}^{33} \end{bmatrix}, \tag{19}$$

where the components of the submatrices \mathbf{K}^{ij} are given by

$$K_{ij}^{11} = \int_{h^e} A_{xx} \frac{d\psi_i^u}{dx} \frac{d\psi_j^u}{dx} dx, \quad K_{ij}^{12} = \int_{h^e} -\kappa E_{xx} \frac{d\psi_i^u}{dx} \frac{d^2\psi_j^w}{dx^2} dx, \quad K_{il}^{13} = \int_{h^e} \hat{B}_{xx} \frac{d\psi_i^u}{dx} \frac{d\psi_l^\phi}{dx} dx,$$

$$K_{Ij}^{21} = K_{Ji}^{12}, \quad K_{IJ}^{22} = \int_{h^e} \left[\kappa^2 H_{xx} \frac{d^2\psi_I^w}{dx^2} \frac{d^2\psi_J^w}{dx^2} + (\hat{A}_{xz} - \beta \hat{D}_{xz}) \frac{d\psi_I^w}{dx} \frac{d\psi_J^w}{dx} \right] dx,$$

$$K_{Il}^{23} = \int_{h^e} \left[-\kappa \hat{F}_{xx} \frac{d^2\psi_I^w}{dx^2} \frac{d\psi_l^\phi}{dx} + (\hat{A}_{xz} - \beta \hat{D}_{xz}) \frac{d\psi_I^w}{dx} \psi_l^\phi \right] dx, \quad K_{kj}^{31} = K_{li}^{13},$$

$$K_{kJ}^{32} = K_{lI}^{23}, \quad K_{kl}^{33} = \int_{h^e} \left[(\hat{D}_{xx} - \kappa \hat{F}_{xx}) \frac{d\psi_k^\phi}{dx} \frac{d\psi_l^\phi}{dx} + (\hat{A}_{xz} - \beta \hat{D}_{xz}) \psi_k^\phi \psi_l^\phi \right] dx,$$

and the resultants are defined as follows:

$$\begin{aligned}
 A_{xx} &= \int_A E(z) dA, & B_{xx} &= \int_A zE(z) dA, & D_{xx} &= \int_A z^2 E(z) dA, \\
 E_{xx} &= \int_A z^3 E(z) dA, & F_{xx} &= \int_A z^4 E(z) dA, & H_{xx} &= \int_A z^6 E(z) dA, \\
 \hat{B}_{xx} &= B_{xx} - \kappa E_{xx}, & \hat{D}_{xx} &= D_{xx} - \kappa F_{xx}, & \hat{F}_{xx} &= F_{xx} - \kappa H_{xx}, \\
 A_{xz} &= \int_A G(z) dA, & D_{xz} &= \int_A z^2 G(z) dA, & F_{xz} &= \int_A z^4 G(z) dA, \\
 \hat{A}_{xz} &= A_{xz} - \beta D_{xz}, & \hat{D}_{xz} &= D_{xz} - \beta F_{xz},
 \end{aligned}$$

where

$$\beta = 3\kappa.$$

Additionally, from the internal virtual work, the thermal force vector is defined as

$$\mathbf{F}_T^e = [{}^T F^1 \quad {}^T F^2 \quad {}^T F^3]^T, \tag{20}$$

where

$${}^T F_i^1 = \int_{h^e} L^T \frac{d\psi_i^u}{dx} dx, \quad {}^T F_I^2 = \int_{h^e} -N^T \frac{d^2 \psi_I^w}{dx^2} dx, \quad {}^T F_k^3 = \int_{h^e} (M^T - N^T) \frac{d\psi_k^\phi}{dx} dx,$$

with

$$\{L^T, M^T, N^T\} = \int_A \{1, z, \kappa z^3\} \alpha(z) E(z) [T(z) - T_{ref}] dA.$$

Now, from the external virtual work, the force vector is given by

$$\mathbf{F}_M^e = [0 \quad {}^M F^2 \quad 0]^T. \tag{21}$$

where

$${}^M F_I^2 = \int_{h^e} q_0 \psi_I^w dx.$$

Finally, the thermo-mechanical finite element model has the following form:

$$\mathbf{K}^e \Delta = \mathbf{F}_M^e + \mathbf{F}_T^e. \tag{22}$$

4. Numerical Results

This section is divided into four parts: a dependence study of η , the validation of the present model to perform static analysis, the validation of the thermal-structural analysis for isotropic beams, and a thermal-structural analysis of FG beams. Due to the lack of models using similar temperature distributions and the rule of mixtures in conjunction with the power law, the behavior of the present model is tested separately.

The results of the second part validate the behavior of the FGM model and allow us to perform a static analysis. The results of the third part validate the behavior of the thermo-mechanical model implemented for isotropic beams, and lastly, we perform a comparison with the numerical results obtained using a commercial software to verify the thermo-mechanical behavior of FG beams.

Unless otherwise specified, the mechanical properties of the constituents of the FG beams we used are presented in Table 1. The top constituent was ceramic.

Table 1. Mechanical properties of the FGM constituents.

Material	E (GPa)	ν	K (W/m ² °C)	α (1/°C)
Aluminum (Al)	70	0.3	204	23×10^{-6}
Alumina (Al ₂ O ₃)	380	0.3	10.4	7.4×10^{-6}

In addition, the geometrical parameters of width and thickness are fixed values, where $b = 1$ m and $t = 1$ m. Thus, it is only needed to vary the length, L , to obtain different length-to-thickness ratios.

4.1. Dependence Study of Parameter η

Recalling that the temperature distribution (see Equation (4)) involves approximations depending on the numbers of terms used in the series (i.e., parameter η) and to achieve the accuracy and independence of η , it is proper to study the influence of this parameter on the results. Table 2 presents the displacements of a clamped-free FG beam under thermal load for several values of the parameter η . When $\eta > 100$, it is noted that the values of both displacements converge. Despite the slight difference in the results, in this work, 100 terms are used to evaluate the temperature distribution.

Table 2. Maximum displacements for a clamped-free FG beam subjected to only thermal load ($L/t = 5$, $T_{top} = 400$ °C, $T_{bot} = T_{ref} = 300$ °C).

η	n = 0.5		n = 1		n = 5	
	$u^0 \times 10^{-3}$	$w^0 \times 10^{-3}$	$u^0 \times 10^{-3}$	$w^0 \times 10^{-3}$	$u^0 \times 10^{-3}$	$w^0 \times 10^{-3}$
10	1.7247	−9.2646	1.9362	−8.9328	3.3252	−10.4942
25	1.4931	−8.7550	1.7070	−8.3815	3.1461	−10.0095
50	1.4283	−8.5021	1.6477	−8.1640	3.0990	−9.8696
100	1.4162	−8.4439	1.6369	−8.1186	3.0906	−9.8436
200	1.4156	−8.4410	1.6365	−8.1165	3.0902	−9.8425
400	1.4156	−8.4410	1.6365	−8.1165	3.0902	−9.8425

4.2. Static Analysis

A static analysis of various FG beams subjected to a distributed load was performed to verify the implementation of the FGM model in the present finite element model. The boundary conditions of the FG beam analyzed were clamped-free (C-F) and simply supported (S-R). Table 3 presents the mechanical properties of the two FGM constituents considered. In addition, it must be noted that the metal or ceramic may be the top or bottom constituent according to the boundary condition to be studied. The latter consideration is made to be consistent with the properties of FGM used in studies reported in the available literature.

Table 3. Mechanical properties of the FGM constituents for static analyses.

Material	E (GPa)	ν	C-F	S-R
Aluminum (Al)	70	0.3	Bottom	Top
Zirconia (ZnO ₂)	200	0.3	Top	Bottom

To compare the results with those available in the literature, the following dimensionless parameter for the transverse deflection was used [14]:

$$\bar{w} = w \frac{E_{Al}}{q_0 L^4} \frac{bt^3}{12} \times 10^3. \tag{23}$$

Note that the values of the dimensionless parameter are only valid for the ceramic constituent considered in this static analysis.

In Tables 4–7, the numerical results of the present finite element model are compared with other formulations. The label Present denotes the results of the present model, the label Plane indicates the results obtained by means of a model made in the commercial software ANSYS using a mesh of PLANE182 elements, and references are used to label the literature results.

Tables 4 and 5 present the dimensionless transverse deflections for a C-F FG beam. The behavior is similar for both length-to-thickness ratios; that is, the nearest values to those of the present model are those reported in the work of Vo et al. [19], and those obtained with the plane model are within a relative error of 0.2% with respect to the present formulation. The similarity of the numerical results to the ones of Vo et al. [19] is expected since the latter were also obtained using a higher-order shear deformation theory.

Table 4. Maximum dimensionless transverse deflection of a C-F FG beam subjected to a uniform load distribution ($L/t = 4$).

Work	n = 0	n = 0.2	n = 1	n = 5	n = 10
Present	46.51490	54.00955	74.33885	94.71622	102.49537
Plane	46.57096	53.96973	74.24512	94.62760	102.51855
Vo et al. [19]	46.51500	54.01125	74.33875	94.71625	102.49625

Table 5. Maximum dimensionless transverse deflection of a C-F FG beam subjected to a uniform load distribution ($L/t = 16$).

Work	n = 0	n = 0.2	n = 1	n = 5	n = 10
Present	43.92621	51.13280	70.50375	88.53483	95.67928
Plane	43.86304	51.15649	70.39235	88.44528	95.62302
Vo et al. [19]	43.92625	51.13375	70.50250	88.53375	95.67875

Now, the dimensionless transverse deflections for S-R FG beams are shown in Tables 6 and 7. It can be noted that the results obtained by means of a higher-order shear deformation theory are very close to those of the present model, i.e., the results of Şimşek [29] and Vo et al. [19]. The numerical results reported by Şimşek [29] were obtained using a model based on the TSDT and the Ritz methods. In comparison with the plane model, the results are within a relative error of 0.83%, which is an acceptable value considering that the formulation of the plane element considers a two-dimensional model.

Table 6. Maximum dimensionless transverse deflection of an S-R FG beam subjected to a uniform load distribution ($L/t = 4$).

Work	n = 0	n = 0.5	n = 1	n = 5	n = 10
Present	15.04884	9.53850	8.36849	6.50747	6.00623
Plane	15.05273	9.54069	8.29951	6.49140	6.02041
Şimşek [29]	15.04922	9.53958	8.36862	6.50755	-
Vo et al. [19]	15.04948	9.53828	8.36823	6.50742	-

Table 7. Maximum dimensionless transverse deflection of an S-R FG beam subjected to a uniform load distribution ($L/t = 16$).

Work	n = 0	n = 0.5	n = 1	n = 5	n = 10
Present	13.14767	8.34089	7.38270	5.78671	5.31468
Plane	13.05415	8.28457	7.32718	5.74005	5.27186
Şimşek [29]	13.14779	8.34180	7.38268	5.78672	-
Vo et al. [19]	13.14714	8.34063	7.38255	5.78672	-

In general, the above comparisons show good agreement with the results reported in the literature, and thus, they validate the behavior of the FGM implemented in the present finite element model and the plane model.

4.3. Thermal–Structural Analysis of Isotropic Beams

In this section, isotropic beams subjected to thermal loads and different boundary conditions are analyzed as a first step to validate the thermal behavior of the present finite element model, as well as the plane model. Therefore, exact solutions of the transverse deflection for isotropic beams are used for comparison; the results of the exact solution are denoted with the label Exact. The exact solutions are reported in [30], and according to the boundary conditions, are as follows:

- For a C-F isotropic beam:

$$w(x) = -\frac{\alpha(T_{top} - T_{bot})}{2t}x^2. \tag{24}$$

- For an S-R isotropic beam:

$$w(x) = -\frac{\alpha(T_{top} - T_{bot})}{2t}(xL - x^2). \tag{25}$$

In this case, an isotropic beam made of aluminum is considered. The temperatures are assumed to be $T_{bot} = T_{ref} = 300\text{ }^\circ\text{C}$ and $T_{top} = 400\text{ }^\circ\text{C}$. Tables 8 and 9 present the maximum transverse deflections of C-F and S-R isotropic beams, respectively, subjected to a thermal load for various length-to-thickness ratios. From these comparisons, it can be noted that the results of the present model are equal to those obtained with the exact solutions for both cases of boundary conditions. However, the PLANE model shows better behavior for long beams subjected to C-F conditions, having a maximum relative error value of 1.95% with respect to the exact solution for a ratio of $L/t = 3$. The PLANE model shows better behavior for short beams ($L/t = 3$) in the case of the S-R condition, where the maximum relative error occurs for a ratio $L/t = 20$ and has a value of 1.50%.

In general, the thermo-mechanical responses for isotropic beams of the present model and the plane model are acceptable.

Table 8. Maximum transverse deflection for C-F isotropic beams subjected to a thermal load for various L/t ratios.

Model	L/t		
	3	5	20
Present	−0.010350	−0.028750	−0.46000
Plane	−0.010552	−0.029037	−0.46027
Exact	−0.010350	−0.028750	−0.46000

Table 9. Maximum transverse deflection for S-R isotropic beams subjected to a thermal load for various L/t ratios.

Model	L/t		
	3	5	20
Present	0.0025875	0.0071875	0.115
Plane	0.0025765	0.0071092	0.11327
Exact	0.0025875	0.0071875	0.115

4.4. Thermal–Structural Analysis of FG Beams

After verifying the performance for the static analysis of FG beams and the thermal–structural analysis of isotropic beams for the present model, the thermo-mechanical re-

sponse of FG beams was examined. For this purpose, the temperatures of the top and bottom surfaces were: $T_{top} = 400\text{ }^\circ\text{C}$, $T_{bot} = 300\text{ }^\circ\text{C}$. Moreover, a uniform distributed load $q_0 = 100\text{ N/m}$ was applied to the FG beam.

The maximum axial displacements and transverse deflections for C-F FG beams with different values of the power law exponent are shown in Table 10. The axial displacement increases as the power law exponent increases; this is a common behavior seen in the mechanical response of FG beams. Conversely, the ceramic volume distribution decreased; however, note that for a value of $n = 1$, the transverse deflection is smaller than the one obtained when $n = 0.5$ due to the presence of the thermal load.

Table 10. Maximum displacements of a C-F FG beam subjected to thermal load and distributed load $q_0 = 100\text{ N/m}$ ($T_{top} = 400\text{ }^\circ\text{C}$, $T_{bot} = 300\text{ }^\circ\text{C}$, and $T_{ref} = 300\text{ }^\circ\text{C}$).

	Model	n = 0.5		n = 1		n = 5		n = 10	
		$u^0 \times 10^{-3}$	$w^0 \times 10^{-3}$						
$L/t = 3$	Present	0.8497	-3.0410	0.9822	-2.9236	1.8544	-3.5354	2.2992	-4.7209
	Plane	0.8514	-3.0958	0.9955	-2.9825	1.9406	-3.6603	2.4064	-4.9210
$L/t = 5$	Present	1.4162	-8.4435	1.6370	-8.1181	3.0906	-9.8428	3.8312	-13.1500
	Plane	1.4182	-8.5175	1.6506	-8.1941	3.1780	-10.0020	3.9411	-13.4360
$L/t = 10$	Present	2.8325	-33.7633	3.2740	-32.4618	6.1814	-39.4007	7.6611	-52.6523
	Plane	2.8356	-33.8830	3.2889	-32.5950	6.2720	-39.7390	7.7786	-53.3280
$L/t = 20$	Present	5.6653	-134.9740	6.5487	-129.7477	12.3642	-157.4974	15.3221	-210.5132
	Plane	5.6725	-134.9600	6.5690	-129.8300	12.4650	-158.3800	15.4580	-212.4600

From the comparisons presented in Table 10, the maximum relative errors are

- $L/t = 3$: 1.98% for $n = 0.5$ and 1, and 4.45% for $n = 5$ and 10, respectively.
- $L/t = 5$: 0.93% for $n = 0.5$ and 1, and 2.79% for $n = 5$ and 10, respectively.
- $L/t = 10$: 0.45% for $n = 0.5$ and 1, and 1.51% for $n = 5$ and 10, respectively.
- $L/t = 20$: 0.31% for $n = 0.5$ and 1, and 0.88% for $n = 5$ and 10, respectively.

It can be observed that most of the above relative errors are below 2.79%, while the maximum values are obtained for a short beam ($L/t = 3$), and $n = 5$ and 10. According to the relative errors obtained, the behavior of the present model is acceptable.

Now, Table 11 presents the maximum axial displacement and transverse deflection for an S-R FG beam with different values of the power law exponent. It is worthwhile to mention that the maximum axial displacement is obtained at $x = L$ and the maximum transverse deflection occurs at $x = L/2$. In comparison with the absolute values of displacement and deflection that the C-F FG beam undergoes for the same mechanical and thermal loads, the transverse deflections are smaller in the S-R FG beam. Moreover, it can be noted that the axial displacements are very similar since the boundary conditions in the axial direction are equal; that is, for an S-R FG beam, the axial displacement at $x = 0$ is restricted, and at $x = L$, it is not, as occurs in the C-F FG beam. However, due to the axial bending coupling generated by the FGM, it is also expected to obtain axial displacements with a small difference between both cases of boundary conditions.

For the results presented in Table 11, the maximum relative errors are

- $L/t = 3$: 2.38% for $n = 0.5$ and 1, and 5.70% for $n = 5$ and 10, respectively.
- $L/t = 5$: 1.39% for $n = 0.5$ and 1, and 3.54% for $n = 5$ and 10, respectively.
- $L/t = 10$: 0.65% for $n = 0.5$ and 1, and 1.89% for $n = 5$ and 10, respectively.
- $L/t = 20$: 0.26% for $n = 0.5$ and 1, and 1.07% for $n = 5$ and 10, respectively.

Note that the maximum relative error is obtained for short beams with higher power law indices, and it is equal to 5.70%. With respect to the second-highest relative error, the values are below 3.54%. Thus, given the above results, the present model can be considered to have an acceptable behavior.

Table 11. Maximum displacements of an S-R FG beam subjected to thermal load and distributed load $q_0 = 100 \text{ N/m}$ ($T_{top} = 400 \text{ }^\circ\text{C}$, $T_{bot} = 300 \text{ }^\circ\text{C}$, and $T_{ref} = 300 \text{ }^\circ\text{C}$).

		n = 0.5		n = 1		n = 5		n = 10	
	Model	$u^0 \times 10^{-3}$	$w^0 \times 10^{-3}$						
$L/t = 3$	Present	0.8496	0.7618	0.9822	0.7320	1.8544	0.8743	2.3005	1.1647
	Plane	0.8299	0.7606	0.9806	0.7324	1.9665	0.8841	2.4383	1.1980
$L/t = 5$	Present	1.4161	2.1125	1.6369	2.0308	3.0906	2.4514	3.8324	3.2722
	Plane	1.3967	2.1124	1.6356	2.0342	3.2037	2.4735	3.9729	3.3271
$L/t = 10$	Present	2.8323	8.4445	3.2738	8.1194	6.1811	9.8449	7.6621	13.1523
	Plane	2.8139	8.4458	3.2736	8.1329	6.2972	9.9199	7.8097	13.3030
$L/t = 20$	Present	5.6646	33.7796	6.5473	32.4830	12.3613	39.4332	15.3207	52.6880
	Plane	5.6500	33.7210	6.5522	32.4700	12.4870	39.6530	15.4860	53.1430

To complement the above numerical results, Figure 2 shows the transverse deflection for various power law exponents of FG beams subjected to thermal and mechanical loads. Figure 2a,b shows the transverse deflection of C-F and S-R FG beams, respectively. For both boundary conditions, the minimum transverse deflection is obtained when $n = 1$.

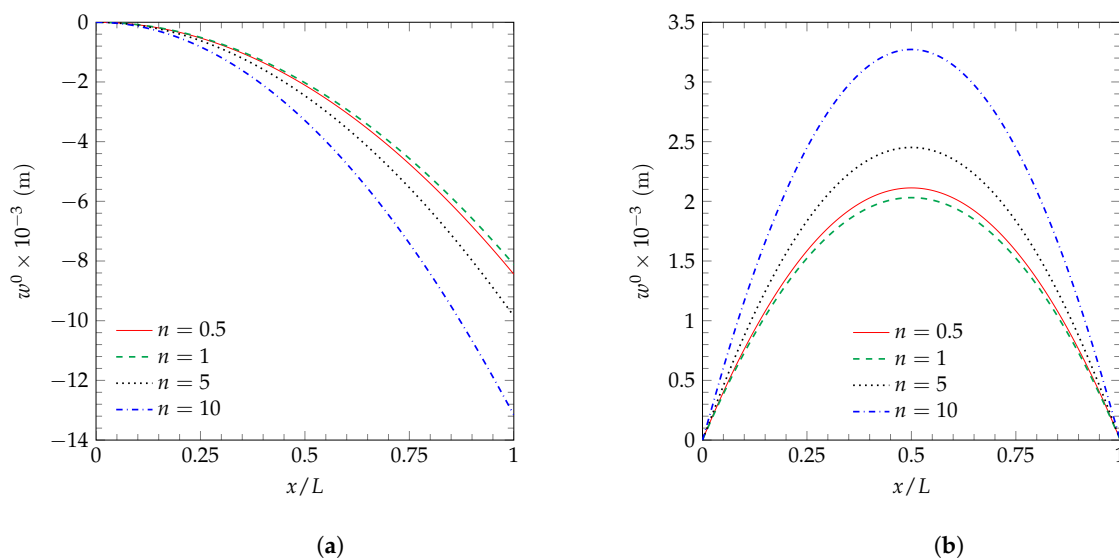


Figure 2. Transverse deflection of various FG beams subjected to thermal and distributed loads where $q_0 = 100 \text{ N/m}$ ($T_{top} = 400 \text{ }^\circ\text{C}$, $T_{bot} = 300 \text{ }^\circ\text{C}$, and $T_{ref} = 300 \text{ }^\circ\text{C}$) under (a) C-F and (b) S-R boundary conditions.

4.5. Thermal–Structural Analysis of FG Beams, for $n = 1$

In this section, the thermo-mechanical response of the FG beam with a power law exponent $n = 1$ is studied for the C-F and an S-R boundary conditions. For this analysis, a distributed load $q_0 = -10^4 \text{ N/m}$ was applied to the FG beam, and the top surface temperature was considered to vary, while the other temperatures remained fixed; that is, the temperature of reference and bottom surface temperature were considered to be constant with the following values: $T_{ref} = 0 \text{ }^\circ\text{C}$ and $T_{bot} = 20 \text{ }^\circ\text{C}$. The latter consideration allowed us to obtain the behavior of the FG beam as it is exposed to various temperature differences between its top and bottom surfaces, such that $\Delta T = T_{top} - T_{ref}$. Moreover, several length-to-thickness ratios were studied.

The maximum axial displacements and transverse deflections for the C-F FG beam are presented in Table 12; also, numerical results obtained using the plane model are included for comparison purposes. The influence of increasing the top surface temperature can be noted as an increment in both displacements, and the maximum displacements are

obtained when $\Delta T = 400\text{ }^\circ\text{C}$. In addition, a plot of the transverse deflection along the x axis of the FG beam is shown in Figure 3a, where greater deflections are observed as the temperature of the top surface increases.

Table 12. Maximum displacements of a C-F FG beam ($n = 1$) subjected to various ΔT and a distributed load $q_0 = -10^4\text{ N/m}$ ($T_{bot} = 20\text{ }^\circ\text{C}$ and $T_{ref} = 0\text{ }^\circ\text{C}$).

L/h	Model	$\Delta T = 100\text{ }^\circ\text{C}$		$\Delta T = 200\text{ }^\circ\text{C}$		$\Delta T = 300\text{ }^\circ\text{C}$		$\Delta T = 400\text{ }^\circ\text{C}$	
		$u^0 \times 10^{-3}$	$w^0 \times 10^{-3}$						
3	Present	1.8938	-1.5267	2.8760	-4.4503	3.8582	-7.3739	4.8403	-10.2976
	Plane	1.9195	-1.5620	2.9150	-4.5445	3.9105	-7.5270	4.9060	-10.5100
5	Present	3.1554	-4.2698	4.7924	-12.3883	6.4293	-20.5069	8.0662	-28.6255
	Plane	3.1814	-4.2973	4.8320	-12.4920	6.4826	-20.6870	8.1332	-28.8810
10	Present	6.3018	-17.6686	9.5756	-50.1384	12.8495	-82.6082	16.1234	-115.0780
	Plane	6.3288	-17.7010	9.6176	-50.3030	12.9060	-82.9060	16.1950	-115.5100
20	Present	12.5308	-80.1733	19.0785	-210.0480	25.6263	-339.9227	32.1740	-469.7974
	Plane	12.5620	-80.1610	19.1300	-210.1200	25.6980	-340.0800	32.2660	-470.0300

The comparisons of the results presented in Table 12 give the following ranges for the relative errors (ϵ_r):

- $L/t = 3$: $1.34 \leq \epsilon_r \leq 2.26\%$.
- $L/t = 5$: $0.64 \leq \epsilon_r \leq 0.88\%$.
- $L/t = 10$: $0.18 \leq \epsilon_r \leq 0.44\%$.
- $L/t = 20$: $0.02 \leq \epsilon_r \leq 0.29\%$.

As noted before, higher values of relative errors are obtained for the C-F FG beam of ratio $L/t = 3$. For moderately short to long beams, the values are below 0.9%. Therefore, the present model shows good behavior for the thermo-mechanical response of FG beams at different temperatures.

Now, regarding the S-R FG beam, the axial displacements and transverse deflections are presented in Table 13. In this case, the similarities with the axial displacements of C-F FG beam are only observed in short beams; notable differences are observed as the length-to-thickness ratio increases. The transverse deflection of the S-R FG beam is shown in Figure 3b, where again greater deflections are observed as the temperature of the top surface increases.

Table 13. Maximum displacements of an S-R FG beam ($n = 1$) subjected to various ΔT and a distributed load $q_0 = -10^4\text{ N/m}$ ($T_{bot} = 20\text{ }^\circ\text{C}$ and $T_{ref} = 0\text{ }^\circ\text{C}$).

L/h	Model	$\Delta T = 100\text{ }^\circ\text{C}$		$\Delta T = 200\text{ }^\circ\text{C}$		$\Delta T = 300\text{ }^\circ\text{C}$		$\Delta T = 400\text{ }^\circ\text{C}$	
		$u^0 \times 10^{-3}$	$w^0 \times 10^{-3}$						
3	Present	1.8943	0.3802	2.8765	1.1122	3.8587	1.8443	4.8408	2.5763
	Plane	1.8927	0.3807	2.8732	1.1131	3.8538	1.8455	4.8343	2.5779
5	Present	3.1577	1.0502	4.7946	3.0809	6.4316	5.1117	8.0685	7.1425
	Plane	3.1563	1.0540	4.7919	3.0882	6.4276	5.1224	8.0632	7.1565
10	Present	6.3199	4.1343	9.5938	12.2529	12.8677	20.3715	16.1416	28.4900
	Plane	6.3194	4.1525	9.5931	12.2840	12.8670	20.4170	16.1400	28.5490
20	Present	12.6762	15.5429	19.2240	48.0127	25.7718	80.4825	32.3195	112.9523
	Plane	12.6790	15.5870	19.2310	48.0440	25.7840	80.5010	32.3370	112.9600

The ranges of relative errors for the results presented in Table 13 are

- $L/t = 3$: $0.06 \leq \varepsilon_r \leq 0.13\%$.
- $L/t = 5$: $0.04 \leq \varepsilon_r \leq 0.36\%$.
- $L/t = 10$: $0.01 \leq \varepsilon_r \leq 0.44\%$.
- $L/t = 20$: $0.01 \leq \varepsilon_r \leq 0.28\%$.

From Tables 12 and 13, it can be observed that the displacements have similar behavior as presented in the static analyses of FG beams; that is, for a larger length-to-thickness ratio, higher displacements and deflections are presented. Furthermore, higher displacements and deflections are obtained as the temperature of the top surface increases, which is expected since the thermal effects also depend on ΔT .

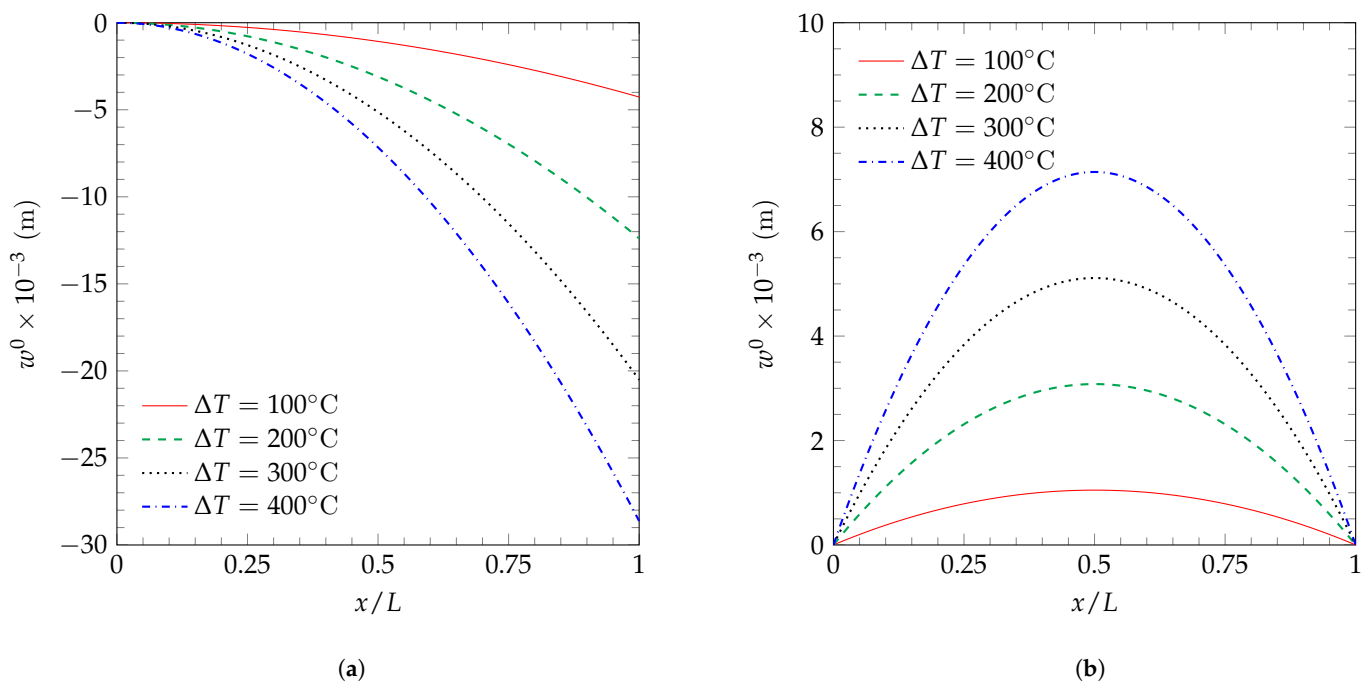


Figure 3. Transverse deflection of FG beams ($n = 1$) subjected to various ΔT and a distributed load $q_0 = -10^4$ N/m ($T_{bot} = 20$ °C and $T_{ref} = 0$ °C) under (a) C-F and (b) S-R boundary conditions.

In addition to the displacements presented in Table 12, the normal stresses through the thickness of a C-F FG beam with $n = 1$ at the clamped end are shown in Figure 4 for the ratios $L/t = 5$ and $L/t = 20$. Additionally, the normal stress obtained by means of the plane model is plotted to compare with the present model’s results; from this comparison, a similar behavior of both models is observed. The normal stress is highly influenced by the length-to-thickness ratio since significant variations are observed in the FG beam with $L/t = 20$. It should be recalled that, in accordance with the temperature distribution and the temperatures considered, higher contributions due to thermal effects are observed at the top surface, where the difference $T(z) - T_{ref}$ reaches its maximum value.

In addition to the results presented in Table 13 for an S-R FG beam with $n = 1$, the variation of the normal stress through the thickness at the mid-span is shown in Figure 5 for the ratios $L/t = 5$ and $L/t = 20$. In the case of S-R conditions, contrary to the C-F condition, a significant influence of the length-to-thickness ratio is not observed on the normal stress.

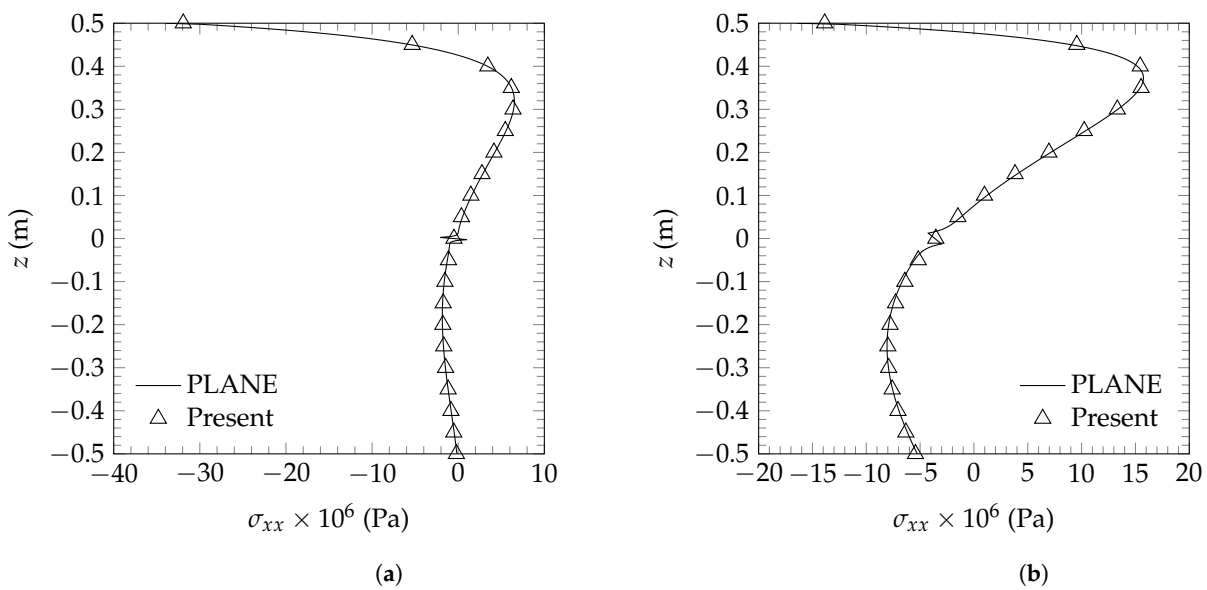


Figure 4. Variation of the normal stress σ_{xx} of a C-F FG beam subjected to a mechanical and thermal load for $n = 1$ and (a) $L/h = 5$; (b) $L/h = 20$ ($q_0 = -10^4$ N/m, $T_{bot} = 20$ °C, and $T_{ref} = 0$ °C).

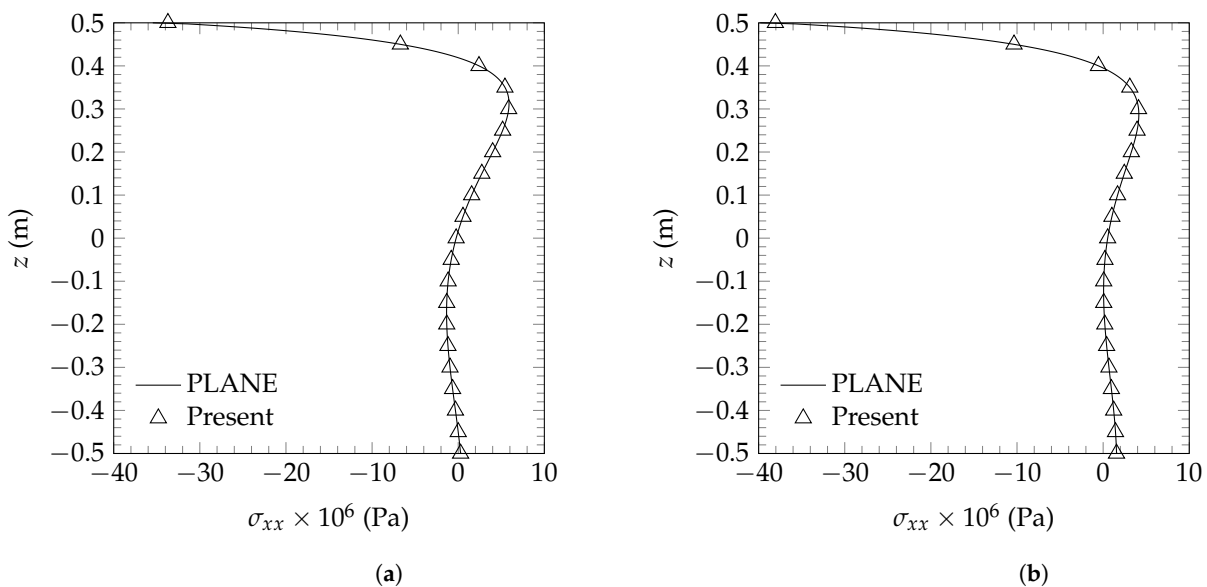


Figure 5. Variation of the normal stress σ_{xx} of an S-R FG beam subjected to a mechanical and thermal load for $n = 1$ and (a) $L/h = 5$; (b) $L/h = 20$ ($q_0 = -10^4$ N/m, $T_{bot} = 20$ °C, and $T_{ref} = 0$ °C).

For completeness, the behavior of the normal stress when $\Delta T = 100$ °C for different values of the power law exponent n and a length to thickness ratio $L/t = 5$ is presented in Figure 6. It can be observed that, the behavior is similar for the C-F and S-R boundary conditions, with the maximum tensile stress being achieved for higher values of n (for the results presented here, it occurs when $n = 10$).

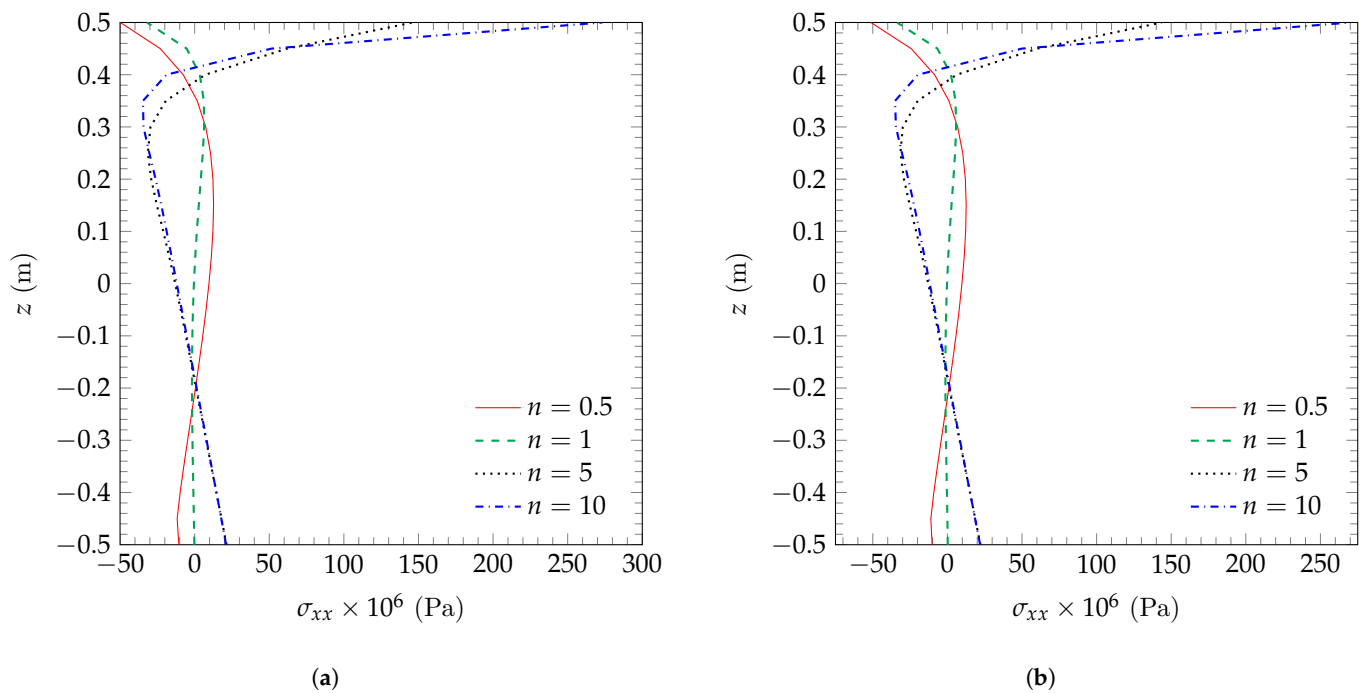


Figure 6. Normal stress (σ_{xx}) of various FG beams subjected to thermal and distributed loads where $q_0 = -10^4$ N/m ($T_{top} = 120$ °C, $T_{bot} = 20$ °C, and $T_{ref} = 0$ °C) under (a) C-F and (b) S-R boundary conditions.

5. Conclusions

In this paper, a finite element model based on TSDT to obtain the thermo-mechanical responses of FG beams subjected to distributed loads and thermal loads was presented. Moreover, the verification of the model's behavior was made in the following order: the mechanical response of FG beams, the thermo-mechanical response of isotropic beams, and, finally, the thermo-mechanical response of FG beams. The latter verification is made by a comparison with the results obtained using plane elements. Slight variations are expected in the comparisons since the formulation of the present model is distinct from the formulations used in the literature and simulations. In general, the following conclusions can be drawn:

- The present finite element model incorporated the rule of mixtures to evaluate the effective mechanical and thermal properties of the FG constituents, where the volume distribution of the ceramic was considered by means of the power law.
- The behavior of the present finite element model was checked by a comparison with the literature and simulations in a finite element commercial code, with the findings showing that the aforementioned results are close to the present ones and behave in a similar manner. Maximum axial displacements and transverse deflections are now available for a comparison with studies that have dealt with the thermal–structural problem presented here.
- In the thermal–structural analysis of FG beams subject to the boundary conditions considered in this article, the higher relative errors were obtained when short beams (e.g., $L/h = 3$) were modeled.
- In addition, we found that normal stresses predicted by the present finite element model were in good agreement with those obtained using plane elements.

Author Contributions: Conceptualization, C.E.V.M. and M.E.G.R.; software, C.E.V.M. and M.E.G.R.; validation, C.E.V.M. and L.D.C.G.; formal analysis, C.E.V.M. and M.E.G.R.; investigation, C.E.V.M. and L.D.C.G.; writing—original draft preparation, C.E.V.M., M.E.G.R. and L.D.C.G.; writing—review and editing, C.E.V.M. and M.E.G.R.; visualization, C.E.V.M. and M.E.G.R. All authors have read and agreed to the published version of the manuscript.

Funding: This research received no external funding.

Data Availability Statement: The data presented in this study are available on request from the corresponding author. The data are not publicly available.

Conflicts of Interest: The authors declare no conflict of interest.

Abbreviations

The following abbreviations are used in this manuscript:

FGM	Functionally graded material
CBT	Classical beam theory
FSDT	First-order shear deformation theory
TSDT	Third-order shear deformation theory
HSDT	Higher-order shear deformation theory
FGB	Functionally graded beams
FG	Functionally graded
L	Beam length
b	Beam width
t	Beam thickness
T_{top}, T_{bot}	Top and bottom surface temperatures
q_0	Uniform distributed load
x, y, z	Rectangular coordinate variables
P	Material property
P_{top}	Top constituent property
P_{bot}	Bottom constituent property
V_{top}	Volume distribution of the top constituent
n	Power law exponent
$K(z)$	Thermal conductivity
K_{top}, K_{bot}	Thermal conductivity of top and bottom constituents
i	Index of the sum
η	Number of terms used in the series for the approximation
u^0, w^0, ϕ^0	Axial displacement, transverse displacement, and rotation of a point located at the centroidal axis x
$(\cdot)^M$	Quantity related to mechanical effects
$(\cdot)^T$	Quantity related to thermal effects
$\varepsilon_{11}, \gamma_{13}$	Axial and transverse strains
$\alpha(z)$	Thermal expansion coefficient
T_{ref}	Temperature of reference
σ_{11}, γ_{13}	Normal and shear stresses
$E(z), G(z)$	Young's and shear moduli
$\nu(z)$	Poisson's ratio
$\delta W_I, \delta W_E$	Internal and external virtual works
\mathbf{f}	Vector of external forces
h_e	One-dimensional domain
ψ	Interpolation functions
\mathbf{K}^e	Element's stiffness matrix
\mathbf{K}^{ij}	Submatrices of element's stiffness matrix
\mathbf{F}_T^e	Element's thermal force vector
\mathbf{F}_M^e	Element's force vector
Al	Aluminum

Al_2O_3	Alumina
C-F	Clamped-free boundary conditions
ΔT	Temperature difference between top surface temperature and reference temperature
S-R	Simply supported boundary conditions
ZnO_2	Zirconia
Present	Numerical results of the present model
Plane	Numerical results of the plane model
Exact	Exact solution results
ε_r	Relative error

References

- Chakraborty, A.; Gopalakrishnan, S.; Reddy, J. A new beam finite element for the analysis of functionally graded materials. *Int. J. Mech. Sci.* **2003**, *45*, 519–539. [\[CrossRef\]](#)
- Elishakoff, I.E.; Pentaras, D.; Gentilini, C. *Mechanics of Functionally Graded Material Structures*; World Scientific: Singapore, 2015.
- Ebrahimi, F.; Jafari, A. A four-variable refined shear-deformation beam theory for thermo-mechanical vibration analysis of temperature-dependent FGM beams with porosities. *Mech. Adv. Mater. Struct.* **2018**, *25*, 212–224. [\[CrossRef\]](#)
- Xia, Y.M.; Li, S.R.; Wan, Z.Q. Bending solutions of FGM Reddy–Bickford beams in terms of those of the homogenous Euler–Bernoulli beams. *Acta Mech. Solida Sin.* **2019**, *32*, 499–516. [\[CrossRef\]](#)
- Mahmood, R.; Jen, T.; Akinlabi, S.; Hassan, S.; Shatalov, M.; Murashkin, E.; Akinlabi, E.T. Functionally Graded Materials: An Introduction. In *Functionally Graded Materials (FGMs)*; CRC Press: Boca Raton, FL, USA, 2021; pp. 1–12.
- Giunta, G.; Crisafulli, D.; Belouettar, S.; Carrera, E. A thermo-mechanical analysis of functionally graded beams via hierarchical modelling. *Compos. Struct.* **2013**, *95*, 676–690. [\[CrossRef\]](#)
- De Pietro, G.; Hui, Y.; Giunta, G.; Belouettar, S.; Carrera, E.; Hu, H. Hierarchical one-dimensional finite elements for the thermal stress analysis of three-dimensional functionally graded beams. *Compos. Struct.* **2016**, *153*, 514–528. [\[CrossRef\]](#)
- Malik, P.; Kadoli, R. Thermo-elastic response of SUS316- Al_2O_3 functionally graded beams under various heat loads. *Int. J. Mech. Sci.* **2017**, *128–129*, 206–223. [\[CrossRef\]](#)
- El-Megharbel, A. A theoretical analysis of functionally graded beam under thermal loading. *World J. Eng. Technol.* **2016**, *4*, 437–449. [\[CrossRef\]](#)
- Li, X.F. A unified approach for analyzing static and dynamic behaviors of functionally graded Timoshenko and Euler–Bernoulli beams. *J. Sound Vib.* **2008**, *318*, 1210–1229. [\[CrossRef\]](#)
- Alshorbagy, A.E.; Eltahir, M.; Mahmoud, F. Free vibration characteristics of a functionally graded beam by finite element method. *Appl. Math. Model.* **2011**, *35*, 412–425. [\[CrossRef\]](#)
- Moheimani, R.; Ahmadian, M.T. On free vibration of functionally graded Euler-Bernoulli beam models based on the non-local theory. In *Vibration, Acoustics and Wave Propagation, Proceedings of the ASME International Mechanical Engineering Congress and Exposition, Houston, TX, USA, 9–15 November 2012*; ASME: New York, NY, USA, 2012; Volume 12, pp. 169–173.
- Nguyen, T.K.; Vo, T.P.; Thai, H.T. Static and free vibration of axially loaded functionally graded beams based on the first-order shear deformation theory. *Compos. Part B Eng.* **2013**, *55*, 147–157. [\[CrossRef\]](#)
- Katili, I.; Syahril, T.; Katili, A.M. Static and free vibration analysis of FGM beam based on unified and integrated of Timoshenko’s theory. *Compos. Struct.* **2020**, *242*, 112130.
- Kadoli, R.; Akhtar, K.; Ganesan, N. Static analysis of functionally graded beams using higher order shear deformation theory. *Appl. Math. Model.* **2008**, *32*, 2509–2525. [\[CrossRef\]](#)
- Aydogdu, M.; Taskin, V. Free vibration analysis of functionally graded beams with simply supported edges. *Mater. Des.* **2007**, *28*, 1651–1656. [\[CrossRef\]](#)
- Mahi, A.; Adda Bedia, E.; Tounsi, A.; Mechab, I. An analytical method for temperature-dependent free vibration analysis of functionally graded beams with general boundary conditions. *Compos. Struct.* **2010**, *92*, 1877–1887. [\[CrossRef\]](#)
- Thai, H.T.; Vo, T.P. Bending and free vibration of functionally graded beams using various higher-order shear deformation beam theories. *Int. J. Mech. Sci.* **2012**, *62*, 57–66. [\[CrossRef\]](#)
- Vo, T.P.; Thai, H.T.; Nguyen, T.K.; Inam, F. Static and vibration analysis of functionally graded beams using refined shear deformation theory. *Meccanica* **2014**, *49*, 155–168.
- Şimşek, M.; Reddy, J.N. Bending and vibration of functionally graded microbeams using a new higher order beam theory and the modified couple stress theory. *Int. J. Eng. Sci.* **2013**, *64*, 37–53.
- Gao, X.L.; Zhang, G.Y. A microstructure- and surface energy-dependent third-order shear deformation beam model. *Z. Angew. Math. Phys.* **2015**, *66*, 1871–1894.
- Chakraborty, A.; Gopalakrishnan, S. A spectrally formulated finite element for wave propagation analysis in functionally graded beams. *Int. J. Solids Struct.* **2003**, *40*, 2421–2448. [\[CrossRef\]](#)
- Daneshmehr, A.R.; Mohammad Abadi, M.; Rajabpoor, A. Thermal effect on static bending, vibration and buckling of Reddy beam based on modified couple stress theory. *Appl. Mech. Mater.* **2013**, *332*, 331–338. [\[CrossRef\]](#)
- Lim, T.K.; Kim, J.H. Thermo-elastic effects on shear correction factors for functionally graded beam. *Compos. Part B Eng.* **2017**, *123*, 262–270. [\[CrossRef\]](#)

25. Praveen, G.N.; Reddy, J.N. Nonlinear transient thermoelastic analysis of functionally graded ceramic-metal plates. *Int. J. Solids Struct.* **1998**, *35*, 4457–4476. [[CrossRef](#)]
26. Javaheri, R.; Eslami, M.R. Thermal buckling of functionally graded plates. *AIAA J.* **2002**, *40*, 162–169. [[CrossRef](#)]
27. Reddy, J.N. On locking-free shear deformable beam finite elements. *Comput. Methods Appl. Mech. Eng.* **1997**, *149*, 113–132. [[CrossRef](#)]
28. Reddy, J.N. *Energy Principles and Variational Methods in Applied Mechanics*; John Wiley & Sons: Hoboken, NJ, USA, 2002.
29. Şimşek, M. Static analysis of a functionally graded beam under a uniformly distributed load by Ritz method. *Int. J. Eng. Appl. Sci.* **2009**, *1*, 1–11.
30. Hetnarski, R.B.; Eslami, M.R. Solid Mechanics and Its Applications. In *Thermal Stresses—Advanced Theory and Applications*; Springer: Dordrecht, The Netherlands, 2009; Volume 158.

Disclaimer/Publisher’s Note: The statements, opinions and data contained in all publications are solely those of the individual author(s) and contributor(s) and not of MDPI and/or the editor(s). MDPI and/or the editor(s) disclaim responsibility for any injury to people or property resulting from any ideas, methods, instructions or products referred to in the content.